ISA Transactions 51 (2012) 208–219

Contents lists available at SciVerse ScienceDirect

ISA Transactions

journal homepage: www.elsevier.com/locate/isatrans

Identification and real-time position control of a servo-hydraulic rotary actuator by means of a neurobiologically motivated algorithm

Ali Sadeghieh [a,*], Hadi Sazgar [b,1], Kamyar Goodarzi [c,2], Caro Lucas [d,e,3]

[a] Faculty of Aerospace Engineering, K.N. Toosi University of Technology, No. 42 Chamran Alley, North Shahin Street, Hemmat Highway west, Tehran 1475883579, Iran
[b] Faculty of Mechanical Engineering, K.N. Toosi University of Technology, P.O. Box: 19395–1999, Tehran, Iran
[c] Faculty of Civil Engineering, Amirkabir University of Technology, P.O. Box: 15875–4413, Tehran, Iran
[d] Center of Excellence for Control and Intelligent Processing, School of Electrical and Computer Engineering, Department of Engineering, University of Tehran, P.O. Box: 14395–515, Tehran, Iran
[e] School of Cognitive Science, IPM, Tehran, Iran

ARTICLE INFO

Article history:
Received 19 February 2011
Received in revised form
9 September 2011
Accepted 12 September 2011
Available online 19 October 2011

Keywords:
Auto-tuned fuzzy PI controller
Brain emotional learning based intelligent controller
Electro-hydraulic servo systems
Neural network predictive controller
Parameter identification
PID controller

ABSTRACT

This paper presents a new intelligent approach for adaptive control of a nonlinear dynamic system. A modified version of the brain emotional learning based intelligent controller (BELBIC), a bio-inspired algorithm based upon a computational model of emotional learning which occurs in the amygdala, is utilized for position controlling a real laboratorial rotary electro-hydraulic servo (EHS) system. EHS systems are known to be nonlinear and non-smooth due to many factors such as leakage, friction, hysteresis, null shift, saturation, dead zone, and especially fluid flow expression through the servo valve. The large value of these factors can easily influence the control performance in the presence of a poor design. In this paper, a mathematical model of the EHS system is derived, and then the parameters of the model are identified using the recursive least squares method. In the next step, a BELBIC is designed based on this dynamic model and utilized to control the real laboratorial EHS system. To prove the effectiveness of the modified BELBIC's online learning ability in reducing the overall tracking error, results have been compared to those obtained from an optimal PID controller, an auto-tuned fuzzy PI controller (ATFPIC), and a neural network predictive controller (NNPC) under similar circumstances. The results demonstrate not only excellent improvement in control action, but also less energy consumption.

1. Introduction

A brief look into various industries can clearly illuminate the widespread and increasing application of electro-hydraulic servo systems. Their possessing a combination of unique characteristics such as high power-to-weight ratio, rapid response, and high bandwidth has resulted in everyday growth in the application of these systems. Lubrication ability and spontaneous heat transfer due to oil properties is another advantage of such mechanisms. Heat transfer over time causes the fluid temperature to rise; consequently, temperature-sensitive factors such as the density, viscosity, and bulk modulus change dramatically. For hydraulic systems operating for long periods of time or under temperature-varied conditions, the variation of these parameters is not negligible and may cause noticeable change in the dynamics of the system [1]. All mentioned factors lead to completely nonlinear and time varied dynamics in hydraulic systems. In a state in which the designed controller is unable to compensate for alterations and ensure desirable performance, the system will become unstable. As these systems are generally under high operating pressures, any form of instability will result in immense pressure fluctuations and may cause severe damage to the system components. Therefore ensuring the smooth operation of the system is an essential point to be considered in designing the controller.

The control algorithms presented can be categorized into three main groups: linear, classic nonlinear, and intelligent. In the process of selecting the type of servo-hydraulic controller, factors such as accuracy, demanded velocity, operating duration, dynamic model accuracy, and external disturbance value should be considered simultaneously.

Linear control algorithms are designed based on a linearized model of the system which is suitable for simple and common

* Corresponding author. Tel.: +98 21 44415695; fax: +98 21 77791045.
E-mail addresses: a.sadeghieh@gmail.com (A. Sadeghieh), hsazgar@gmail.com (H. Sazgar), kamyar.goodarzi@gmail.com (K. Goodarzi), lucas@ut.ac.ir (C. Lucas).
[1] Tel.: +98 21 77193193.
[2] Tel.: +98 21 44410919.
[3] Tel.: +98 21 88141271.

0019-0578/$ – see front matter © 2011 ISA. Published by Elsevier Ltd. All rights reserved.
doi:10.1016/j.isatra.2011.09.006

Nomenclature

A_i	Amygdala nodal output.
A_{sv}	Servo valve orifice opening area (m^2).
B	Viscous damping coefficient (N m s).
C_d	Discharge coefficient.
C_L	Leakage coefficient ((m^4 s)/kg).
D_m	Actuator displacement (m^3/rad).
E	BEL model overall output.
E'	BEL model overall output (except thalamus signal).
e	Control reference error (rad).
J_t	Actuator and load inertia (kg m^2).
K_{sv}	Servo valve constant gain (m^2/Volt).
O_i	Orbitofrontal cortex nodal output.
$P_{c1,c2}$	Pressure in actuator chambers (Pa).
P_L	Load pressure (Pa).
P_s	Supply pressure (Pa).
$Q_{c1,c2}$	Flow rate in/out of actuators (m^3/s).
REW	Emotional signal.
S_i	Sensory input signal.
S_{th}	Thalamus signal.
t	Time (s).
u	Servo valve control input (Volt).
V_i	Amygdala adaptive gain for node i.
V_0	Oil volume under compression (m^3).
W_i	Orbitofrontal cortex adaptive gain for node i.
y_p	Plant output (rad).
y_r	Reference output (rad).
α_a	Amygdala learning rate.
α_o	Orbitofrontal cortex learning rate.
β	Fluid bulk modulus (Pa).
ρ	Fluid mass density (kg/m^3).
θ	Actuator angular position (rad).
$\dot{\theta}$	Actuator angular speed (rad/s).
τ_{sv}	Servo valve time constant (s).

applications [2]. This fact will impose certain limitations on the operating range and control accuracy.

Results obtained from classic nonlinear control algorithms such as sliding mode [3,4], feedback linearization [5], backstepping [6], and robust H-infinity [7] compared to those from linear algorithms are considerably more satisfactory. The major difficulty is extracting an accurate dynamic model of the main system in order to explain the system behavior in the presence of noise and structural uncertainties. Regularly implementation of a nonlinear controller (e.g., sliding mode) in practice is fairly difficult due to the necessity of the measurement of system states and their derivatives.

Intelligent control is widely considered due to high flexibility in selecting the control parameters and feedback, and not requiring a highly accurate dynamic model of the system. These algorithms can be based upon intelligent biological systems. Neural networks and fuzzy logic are examples of this category.

Using linguistic variables, fuzzy control possesses important features such as robustness, approximation ability, and independence to a detailed dynamic model and is capable of generating any demanded nonlinear control behavior. However, a large number of fuzzy rules in high-order systems result in intricate analysis. Sporadically, the computational burden of these controllers, especially in defuzzification step inferences like Mamdani inference, rises significantly.

The learning and adaption ability of neural networks has transformed them into powerful tools for complex applications such as electro-hydraulic servo (EHS) systems. A common problem in most neural networks is that a certain range of input–output information should be previously available. However, granularity of the data may also cause other difficulties. In addition to the prior problem, the dependence of most neural network controllers on the initial values of the neural network weights is also a disadvantage.

One of the recently introduced methods of intelligent control is the brain emotional learning based intelligent controller (BELBIC), which is based upon a computational model of emotional learning algorithms in the human brain. In this paper, a modified version of a BELBIC that mimics a neurologically inspired computational model of the amygdala and the limbic system is introduced. With a brief glance at previously conducted research in this field [8–11], interesting features such as straightforward control structure, learning ability and online adaptation, low online computational load, and not requiring preknowledge of the systems dynamics can be observed. All the above applications of the BELBIC were done in software simulation environments. Prior success in real-time physical implementations of a BELBIC, reported in [12–14], the latter being the only case having industrial application, motivated us to apply the method, for the first time, for angular position control of a laboratorial servo-hydraulic system in order to evaluate its ability in controlling complex industrial systems.

The outline of the paper is as follows. In Section 2, after introducing the computational model related to the emotional learning algorithm in the human brain, the intelligent controller mechanism based upon this type of learning will be comprehensively explained. Dynamic modeling of the EHS system will be thoroughly described in Section 3. Section 4 deals with identification algorithms of the system parameters. Section 5 contains a brief description of the electro-hydraulic workbench used to implement the real-time work. Details of the design process of the BELBIC are put forward in Section 6. In Section 7, the presentation of experimental identification results is followed by a comparison of the experimental results obtained from applying a BELBIC on a real plant with those from use of an optimized PID controller, an auto-tuned fuzzy PI controller (ATFPIC), and a neural network predictive controller (NNPC). Details of PID controller, NNPC, and ATFPIC have been presented in Appendices A–C. Finally, conclusions and remarks bring this work to a close in Section 8.

2. Computational model of a brain emotional learning (BEL) algorithm in the amygdala

Newly conducted studies indicate that emotions are significantly responsible for forming human behavior and decision making in various situations [15]. In a biological system, emotional reactions are applied for quick decision making in complex circumstances and emergency conditions. Humans are creatures renowned for emotional behavior. The process of emotional decision making, which normally occurs rapidly, aids humans to survive perilous situations [16]. It has also been remarked that emotions can play a great role in developing intelligence and learning in humans [17]. For such reasons, many believe that emotion is an undetachable component in machines or systems which imitate intelligent human behavior. Therefore, many studies have been carried out on modeling emotions and the functionality of these models in creating intelligence in machines [18,19]. Emotions are commonly believed to be connected to the limbic part of the brain. The limbic system is presumed to be an evolutionary old part of the brain involved in the survival of the individual and species.

A simple but effective computational model of the emotional learning scheme in the amygdala has recently been developed by Moren and Balkenius [20]. The model introduced aims to regenerate fairly similar characteristics of the biological system by presenting a neurologically inspired computational model of the amygdala and the orbitofrontal cortex (OFC).

The inputs of this brain emotional learning (BEL) model are the sensory input and reward signal, and the output is the emotional decision signal. The BEL model consists of four main parts. The functionality of these parts is described further on.

The thalamus, which preprocesses input signals, is a simplified model of the real thalamus. This part can act as a simple identity function or a filter for reducing noise.

The sensory cortex receives input signals from the thalamus and it is assumed to be responsible for subdividing and discrimination of the coarse input from the thalamus [20].

The orbitofrontal cortex is supposed to inhibit inappropriate responses from the amygdala. In other words, it prevents transient emotional reactions, based on long-term knowledge.

The amygdala is a small structure in the medial temporal lobe of the brain that is responsible for emotional stimulation against input stimuli. This evaluation is in turn used as a basis for emotional states and emotional reactions, and is used for providing attention signals and laying down long-term memories [21].

In this computational model, the amygdala and the orbitofrontal cortex are network structured such that each contains a node for every sensory input. An additional node exists in the amygdala particularly for the signal received from the thalamus. The amount of this signal equals the maximum quantity of sensory inputs.

$$S_{th} = \max_i(S_i). \tag{1}$$

The values for nodes in the amygdala and orbitofrontal cortex are calculated with Eqs. (2) and (3), respectively.

$$A_i = S_i.V_i \tag{2}$$

$$O_i = S_i.W_i. \tag{3}$$

A_i and O_i are, respectively, the node outputs in the network structure of the amygdala and orbitofrontal cortex (OFC), V_i and W_i are weights of the plastic connection in the amygdala and OFC, respectively, and S_i is the sensory input signal. Variations in V_i and W_i during the learning process are estimated by Eqs. (4) and (5).

$$\Delta V_i = \alpha_a\left(\max\left[0, S_i\left(REW - \sum_j A_j\right)\right]\right) \tag{4}$$

$$\Delta W_i = \alpha_o(S_i(E' - REW)), \tag{5}$$

where

$$E' = \sum_i A_i - \sum_i O_i \quad (\text{except } S_{th}). \tag{6}$$

α_a and α_o are amygdala and orbitofrontal learning rates, respectively. Adjusting these parameters determines the learning duration. It should be noted that *REW* is the punishment or stress signal.

The term max (in Eq. (4)) is for making the learning changes monotonic, implying that the amygdala gain can never be decreased. At first glance, this may seem like a fairly substantial drawback; however, there are sufficient reasons for this design choice. Once an emotional reaction has been learned, this should be permanent. It is the task of the orbitofrontal part to inhibit this reaction when it is inappropriate [21]. In earlier versions of a BELBIC [22], where a simplified version of emotional learning algorithm was employed, the sensory input signals were ignored in updating the amygdala and OFC weights in Eqs. (4) and (5). Even the later modified versions [8–14] intending to consider sensory input signals, have placed the term S_i outside the *max* function, which in some cases as a result of a negative S_i, may cause a decrease in the amygdala gain, hence defying the previously presented monotonic learning law. The orbitofrontal learning rule is very similar to the amygdala rule. The major difference is that the

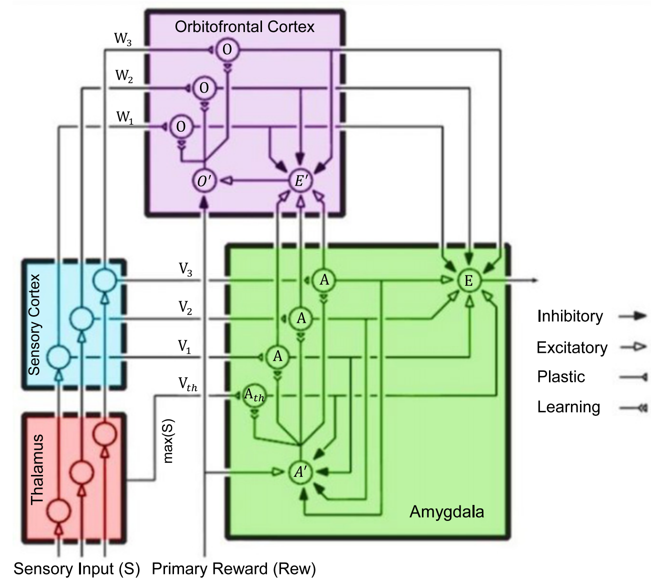

Fig. 1. A graphical depiction of the brain emotional learning process [21].

OFC connection weight can either increase or decrease as needed to track the required inhibition that is reflected as the discrepancy between the reinforcing signal (*REW*) and E' node. The final output of the model is calculated by the following equation:

$$E = \sum_i A_i - \sum_i O_i \quad (\text{including } S_{th}). \tag{7}$$

A finely detailed schematic figure of the mentioned learning process is shown in Fig. 1. The system operation consists of two levels: the amygdala learns to predict and react to a given reinforcement signal. This subsystem cannot unlearn a connection. The incompatibility between predictions and actual reinforcement signals causes inappropriate responses from the amygdala. The OFC learns to prevent the system output if such mismatches occur.

The Moren and Balkenius model of emotional learning for engineering applications aiming at intelligent-adaptive control of dynamic systems was initially introduced by Lucas et al. [22]. In the leading research carried out by Lucas et al., an adaptive control strategy called a brain emotional learning based intelligent controller (BELBIC) was extracted from the previously developed emotional learning model by Moren and Balkenius.

In the implementation of a BELBIC it should be pointed out that, since this model has originally been proposed for descriptive purposes with no control engineering intention, the model is basically an open loop. In order to use this model as a controller, the designer should obtain sensory inputs and reinforcing signals according to control engineering requirements fed back from system responses.

The *REW* signal is externally provided for the model, and the BELBIC attempts to change the weights in order to reduce the *REW* signal. The reinforcing signal (*REW*) comes as a function of other signals which can be supposed as a cost function validation. Specifically, reward (or punishment) is applied based on a previously defined cost function:

$$REW = J(S_i, e, u). \tag{8}$$

The choice of external reinforcement signal provides a degree of freedom for multi-objective learning procedures. Similarly, the sensory inputs can be a function of plant and controller outputs as follows:

$$S = \underline{f}(u, e, y_p, y_r), \tag{9}$$

where $\underline{f}$ is a vector.

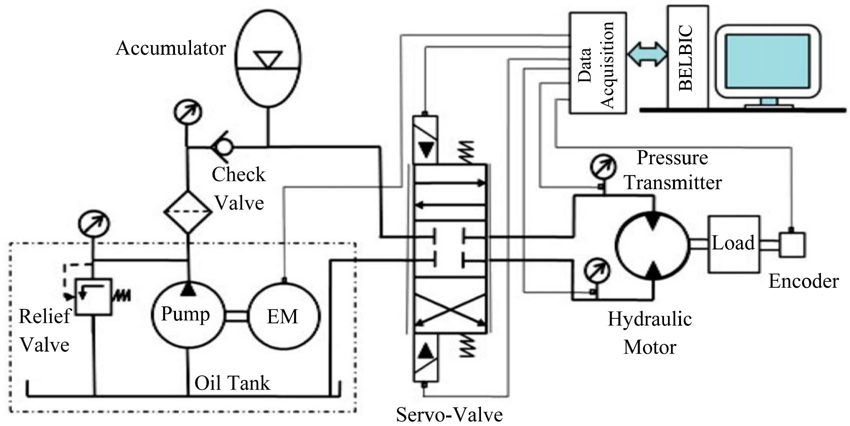

Fig. 2. Schematic diagram of the experimental set-up.

As is illustrated in Eqs. (8) and (9), the sensory input and the reward signal could be arbitrary functions of the reference output (y_r), the plant's output (y_p), the control effort (u), and the error signal (e). In general, it is up to the designer to find a proper set-up for the reward signal and sensory input functions for the BELBIC. The BELBIC stability is discussed using a cell-to-cell mapping method, explained in [23]; also, in order to ensure stability of the system, a general idea for choosing control parameters is given in [23].

3. System dynamics modeling

A symbolic representation of the applied rotary electro-hydraulic servo system is suggested in Fig. 2. The angular position of the hydro motor is controlled as follows. After the actual angular position is measured by the encoder and compared to the desired value, an appropriate control signal is determined and transmitted to the servo valve. The pressure on both chambers of the hydro motor is conveniently adjusted to the control signal by the valve. Applicable tuning of these pressures enables the angular position of the hydro motor to be controlled.

Extraction of dynamic equations of the valve is the most complicated step of modeling a servo-hydraulic system. The applied valve is a two-stage flapper–nozzle valve which includes three main parts: an electrical torque motor, hydraulic amplifier, and valve spool assembly. A schematic view of the hydro motor in addition to the valve is given in Fig. 3.

As is highlighted in Fig. 3, a positive current difference (i.e., $i_1 > i_2$) causes a torque on the flapper which moves it to the left, increasing pressure P_1 and decreasing P_2. The spool then moves to the right and continues to move until the torque on the flapper (armature) due to the feedback spring balances the torque due to the input current. At this point, the flapper is approximately centered between the nozzles, but the spool has taken a new position directly proportional to the input current. Considering the nonlinear nature of fluid flow crossing the orifices and the complex dynamics of each valve component (Fig. 3) to provide a precisely accurate model in order to describe the dynamics would be extremely difficult [24]. Furthermore, even if such a model were to be presented, identification and determining the parameters would be far more complex [25]. Since the applied controller described here (due to its quick learning ability) is not dependent on an accurate model, a common model has been used for the valve.

Servo valve modeling can be divided into two levels: dynamic modeling of the fluid flow crossing the valve and valve spool modeling. The dynamics of the valve spool with no noticeable

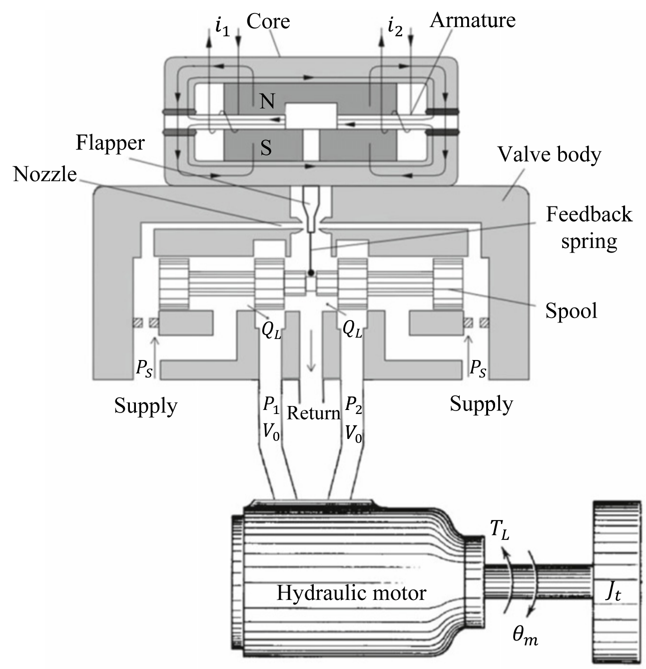

Fig. 3. Construction of the hydraulic servo valve connected to a motor with inertia load.

decline in accuracy in a vast range of frequencies can be described through a first-order transfer function between the valve opening area (A_{sv}) and control input (u) [1]:

$$\tau_{sv}\dot{A}_{sv} + A_{sv} = K_{sv}u, \tag{10}$$

where K_{sv} is the servo valve gain and τ_{sv} is the servo valve time constant. The constants mentioned can be determined from the manufacturer's catalog or by certain tests. Due to the fact that the input of the valve is an electric current but the interface card output is in the form of an electric voltage it is common to use a current to voltage converter. The constant of this converter is considered in the servo valve gain coefficient (K_{sv}).

For an ideal critical center servo valve with a matched and symmetric orifice, the input/output flow rate from the servo valve through the orifices (assuming negligible leakage) can be expressed in the following form:

$$Q_L = C_d A_{sv}\sqrt{\frac{P_s - P_L sign(A_{sv})}{\rho}}, \tag{11}$$

where $P_L = P_{c1} - P_{c2}$ is load pressure or pressure difference between both chambers, $P_s = P_{c1} + P_{c2}$ is the supply pressure and Q_L is the load flow. Assuming no external leakage, Q_L can be considered as the average flow in each path: $Q_L = (\frac{Q_{c1}+Q_{c2}}{2})$, where Q_{c1} and Q_{c2} are the flow rates to and from the servo valve.

C_d and ρ in Eq. (11) indicate the flow discharge coefficient and fluid density, respectively. The *sign* function in Eq. (11) stands for the change in the direction of fluid flow through the servo valve. Employing the compressibility equation for the fluid flow in the actuator dynamics along with the oil leakage will result in the following expression:

$$\frac{V_0}{2\beta}\dot{P}_L = C_d A_{sv}\sqrt{\frac{P_s - P_L sign(A_{sv})}{\rho}} - D_m\dot{\theta} - C_L P_L, \tag{12}$$

where β and V_0 are, respectively, the fluid bulk modulus and oil volume under compression in one chamber of the actuator. D_m and C_L represent the actuator volumetric displacement and total leakage coefficient, respectively. By applying Newton's second law for rotary motion of a hydraulic actuator and neglecting the Coulomb frictional torque,

$$J_t\ddot{\theta} = D_m P_L - B\dot{\theta}, \tag{13}$$

where B is the viscous damping coefficient and J_t is the total inertia of the motor and load referred to the motor shaft.

By combining Eqs. (10)–(13), and by defining the state variables as $x_1 = \theta, x_2 = \dot{\theta}, x_3 = P_L$, and $x_4 = A_{sv}$, a fourth-order nonlinear state space dynamic model can be derived:

$$\begin{cases} \dot{x}_1 = x_2 \\ \dot{x}_2 = w_1x_3 - w_2x_2 \\ \dot{x}_3 = p_1x_4\sqrt{P_s - x_3 sign(x_4)} - p_2x_3 - p_3x_2 \\ \dot{x}_4 = -r_1x_4 + r_2u, \end{cases} \tag{14}$$

where x_1 is the hydro motor angular position (rad), x_2 is the hydro motor angular velocity (rad/s), x_3 is the load pressure (Pa), and x_4 is the valve opening area (m^2). w_1, w_2, p_1, p_2, p_3, r_1, and r_2 are constants, given by

$$\begin{aligned} &w_1 = \frac{D_m}{J_t}, \qquad w_2 = \frac{B}{J_t} \\ &p_1 = \frac{2\beta C_d}{V_0\sqrt{\rho}}, \qquad p_2 = \frac{2\beta C_L}{V_0}, \qquad p_3 = \frac{2\beta D_m}{V_0} \\ &r_1 = \frac{1}{\tau_{sv}}, \qquad r_2 = \frac{K_{sv}}{\tau_{sv}}. \end{aligned} \tag{15}$$

A dynamic model of the system is now extracted, and the parameter values of Eq. (14) should be identified. In the following section, the parameter identification algorithm is provided.

4. System identification algorithm

As mentioned above, some system parameters vary with time. In this section, a continuous recursive least square method has been used in order to identify instant values of these parameters. In state (14), the fourth equation parameters (r_1 and r_2), which are dynamic characteristics of the servo valve spool, can be determined from the manufacturer's guide book. Therefore the only parameters that need to be identified will be present in equations two and three of the dynamic model (Eq. (14)). These equations are rewritten according to Eq. (16):

$$\begin{cases} \dot{x}_2 = w_1x_3 - w_2x_2 \\ \dot{x}_3 = p_1x_4\sqrt{P_s - x_3 sign(x_4)} - p_2x_3 - p_3x_2. \end{cases} \tag{16}$$

Eq. (16) can be rewritten in matrix form as

$$\begin{pmatrix} \dot{x}_2 \\ \dot{x}_3 \end{pmatrix} = \begin{bmatrix} x_3 & -x_2 & 0 & 0 & 0 \\ 0 & 0 & x_4\sqrt{P_s - x_3 sign(x_4)} & -x_3 & -x_2 \end{bmatrix} \times \begin{pmatrix} w_1 \\ w_2 \\ p_1 \\ p_2 \\ p_3 \end{pmatrix}. \tag{17}$$

As Eq. (17) shows, the system has linear parameters; therefore, the continuous recursive least square method with constant trace may be used. Now, let

$$\begin{aligned} &y(t) = \begin{Bmatrix} \dot{x}_2 \\ \dot{x}_3 \end{Bmatrix}, \\ &\varphi^T(t) = \begin{bmatrix} x_3 & -x_2 & 0 & 0 & 0 \\ 0 & 0 & x_4\sqrt{P_s - x_3 sign(x_4)} & -x_3 & -x_2 \end{bmatrix}, \\ &\theta(t) = \begin{pmatrix} w_1 \\ w_2 \\ p_1 \\ p_2 \\ p_3 \end{pmatrix}. \end{aligned} \tag{18}$$

Then:

$$y(t) = \varphi^T(t)\theta. \tag{19}$$

Eq. (19) is a classic form of a system that has an LP (linear in parameters) structure. In this equation, $y(t)$ is the observed vector of variables, $\varphi(t)$ is the matrix of regression variables, and θ is the vector of unknown parameters. Now, the objective function $V(\theta)$ should be minimized, and the matrix $R(t)$ is defined by relations (20) and (21), respectively [26]:

$$V(\theta) = \int_0^t e^{-\alpha(t-s)}[y(s) - \varphi^T(s)\theta]^2\, ds, \quad \alpha \geq 0 \tag{20}$$

$$R(t) = \left(\int_0^t e^{-\alpha(t-s)}\varphi(s)\varphi^T(s)\, ds\right). \tag{21}$$

In Eq. (20), α is the forgetting factor. $V(\theta)$ presents a time-varying weighting of the data. The most recent data (at time t) is given unit weight, but the data at time s is weighted by $e^{-\alpha(t-s)}$.

By defining $P(t) = R(t)^{-1}$ and supposing that matrix $R(t)$ is invertible, the estimated parameter vector which minimizes $V(\theta)$ should satisfy (22) [26]:

$$\begin{aligned} &\frac{d\widehat{\theta}}{dt} = P(t)\varphi(t)e(t) \\ &e(t) = y(t) - \varphi^T(t)\widehat{\theta}(t) \\ &\frac{dP(t)}{dt} = \alpha P(t) - P(t)\varphi(t)\varphi^T(t)P(t). \end{aligned} \tag{22}$$

Finally, (22) verifies the unknown parameters of the system every moment and would lead to attaining the complete dynamic equations of the system.

5. Experimental workbench and settings

Fig. 4 displays the layout of the previously mentioned parts in the applied laboratorial EHS system. The commands issued from the computer within MATLAB-Simulink software environment using C S-Function blocks will be forwarded to the servo valve by a 12-bit interface card. The sampling time during the system identification and control is set to 1 ms. Using an accumulator will stabilize the supply pressure. The maximum working pressure and relief valve threshold is set to 110 bar in all tests. The angular position of the hydro motor is measured by an encoder placed at the end of the shaft.

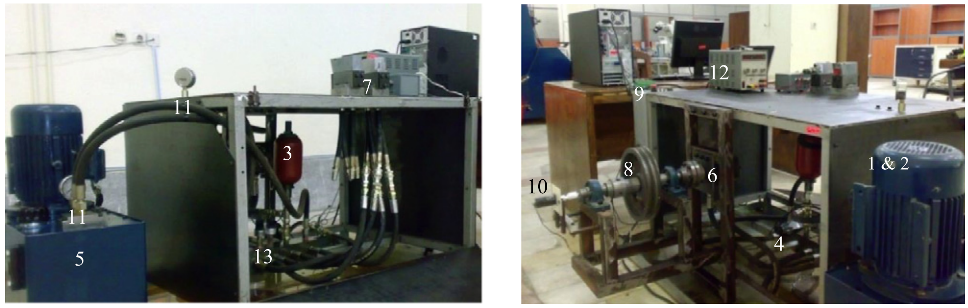

Fig. 4. Experimental EHS system workbench: 1—electric motor; 2—pump; 3—accumulator; 4—relief valve; 5—tank; 6—rotary hydraulic actuator; 7—two-stage servo valve; 8—load; 9—interface card; 10—encoder; 11—pressure sensors; 12—electric power supply; 13—pressure transmitter.

6. Design procedure of the angular position controller

In this section, the controller design procedure is explained in order to control the angular position of the laboratorial rotary EHS system according to the intelligent control algorithm introduced in Section 2.

The controller is bound to issue an appropriate control command to shift the servo valve spool, so that it creates the expected pressure behind the hydro motor in order to track the reference angular position signal instantly. As previously mentioned, the BELBIC must be provided with a set of sensory input signals in addition to a reward signal according to a certain problem. The sensory input, as given in Eq. (23), involves three signals:

$$S = \left[\int |u|^2 dt \; 0.8 y_r \; 2.5 e_\theta \right]^T . \tag{23}$$

The three selected signals related to the sensory inputs which are chosen for the design of the controller include the time integral of the square of the commanded signal u (the very voltage output signal from the controller), the reference signal y_r (the same angular position command θ_d), and the tracking error signal e_θ ($e_\theta = \theta_d - \theta_m$, where θ_m is the measured angular position signal). The coefficients are chosen by trial and error. The intention of the term $\int u$ is to minimize the energy consumption (control effort) of the BELBIC.

The reward or stress signal is created based on control task objectives. The reward function Eq. (24) is similar to a proportional–integral control scheme seeking a suitable tradeoff between quick error adjustment and long-term elimination of the steady-state error.

$$REW = \left(750 e_\theta + 230 \int e_\theta \, dt \right) . \tag{24}$$

It must be noticed that this reward (stress) function can be changed, and for this experiment the presented reward function is appropriate. The amygdala and orbitofrontal cortex learning rates are set equal to $\alpha_a = 4e - 4$ and $\alpha_o = 7e - 3$, respectively. The reason for this selection is to make the orbitofrontal cortex learn the error in the amygdala faster than the amygdala itself to eliminate the error. The general implemented design of the BELBIC controller on the laboratorial EHS system is displayed in Fig. 5. The art of the designer is required to cope appropriately with choosing the system's emotional condition and tune the learning rates of the system itself, to obtain the desired goal.

7. Experimental results and discussion

7.1. Outcome of system identification

The input voltage for identifying the system parameters is a combination of several sinusoidal signals with similar amplitude and different frequencies, and is shown in Fig. 6.

Table 1
Identified parameters of the EHS system.

Parameter	Value	Unit
$w_{1,ave}$	9.61×10^{-5}	m/kg
$w_{2,ave}$	2.56	1/s
$p_{1,ave}$	1.91×10^{10}	$kg^{1/2}/(m^{5/2}\,s^2)$
$p_{2,ave}$	7.92	1/s
$p_{3,ave}$	6.00×10^{6}	$kg/(m\,s^2)$

Table 2
Physical parameters obtained from manufacturer's catalogs.

Parameter	Value	Unit
D_m	7.0×10^{-6}	m^3/rad
K_{sv}	3.0×10^{-6}	m^2/V
τ_{sv}	0.01	s
ρ	850	kg/m^3
β	1.10×10^{-9}	Pa

Table 3
Calculated physical parameters of the EHS system.

Parameter	Value	Unit
V_0	2.6×10^{-3}	m^3
C_d	0.65	–
J_t	7.3×10^{-2}	$kg\,m^2$
B	0.19	N m s
C_L	9.25×10^{-12}	$(m^4\,s)/kg$

The applied sensors in the system consist of two pressure sensors for measuring the pressure at both ends of the hydro motor and an encoder to determine the hydro motor's angular position. x_2, $\dot{x}_2$, and $\dot{x}_3$ are quantitative, calculated by derivation and filtering of the signals measured by the sensors. Since data acquired from sensors, specially the pressure sensors, are always noisy, appropriate filters are required to reduce or eliminate the noise. The filter employed is a first-order low-pass Butterworth filter with the pass band frequency of 50 (rad/s). The identification results of parameters of Eq. (14) in addition to their average values are presented in Fig. 7.

Average values of the identified parameters are provided in Table 1.

The installed E062-433 series servo valve is manufactured by MOOG. The hydro motor applied is a production of "M+S HYDRAULIC" and MLHR series. The hydro motor constants, servo valve, and hydraulic oil properties are shown in Table 2.

Referring to previously mentioned values and Eq. (15), the values of other physical parameters are calculated and shown in Table 3. It should be noted that the values in Table 3 are calculated based on the average parameter results from Table 1.

It is important to include the fact that the purpose of modeling and identification is only providing a dynamic model for offline adjustment of the controller parameters. Online adjustment of the

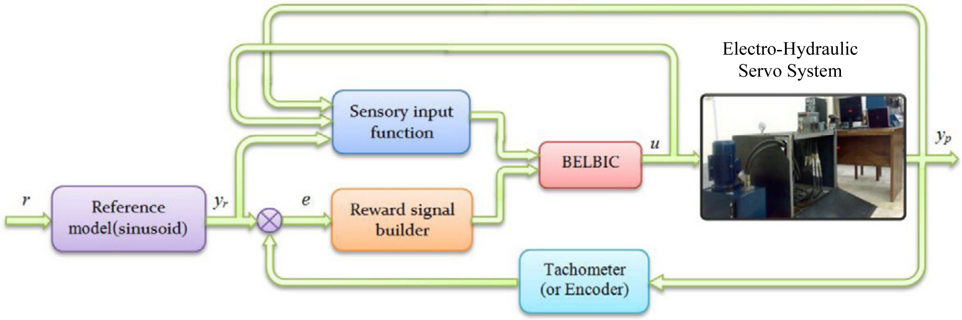

Fig. 5. System configuration using the brain emotional controller.

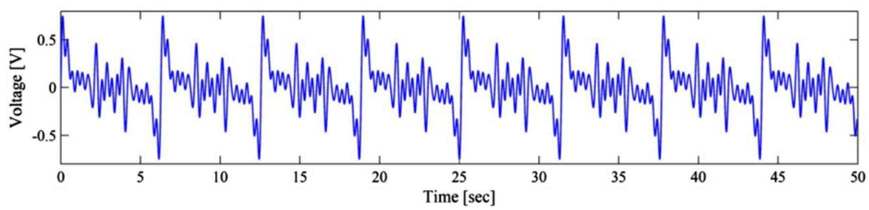

Fig. 6. Input voltage for system identification.

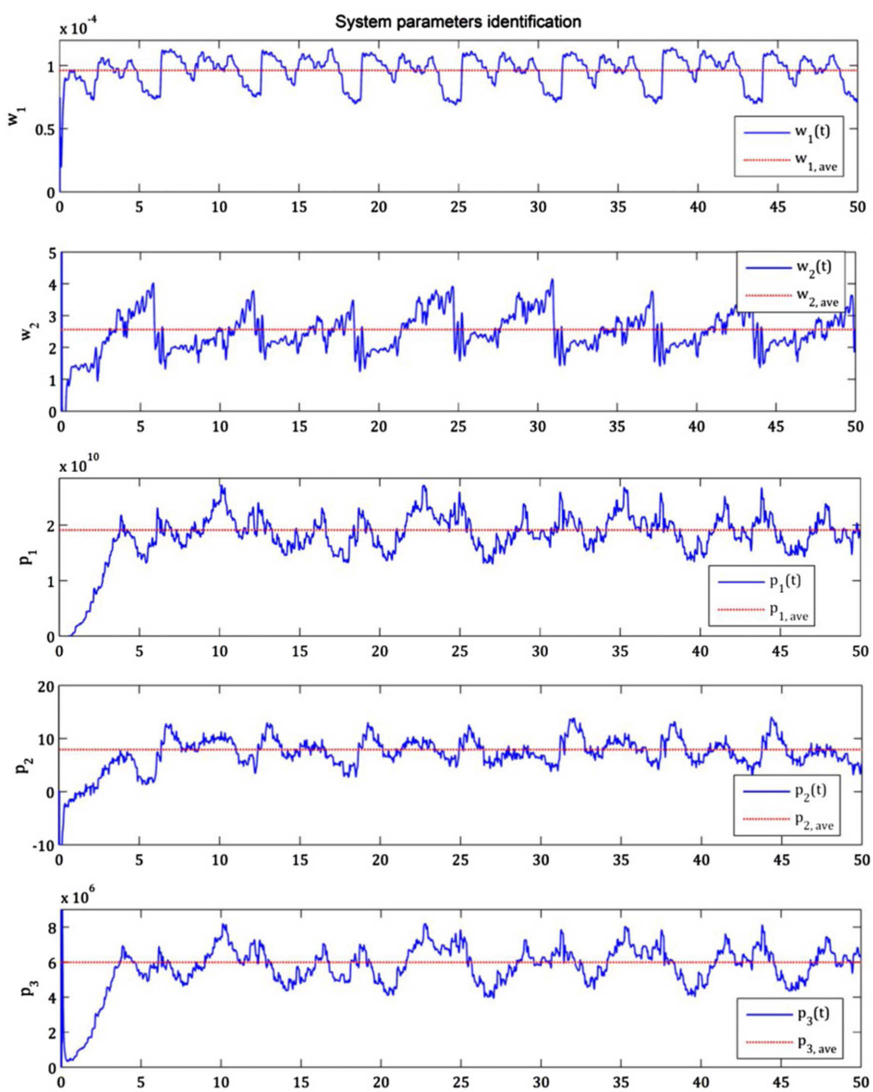

Fig. 7. Identification results of system parameters in addition to their average values.

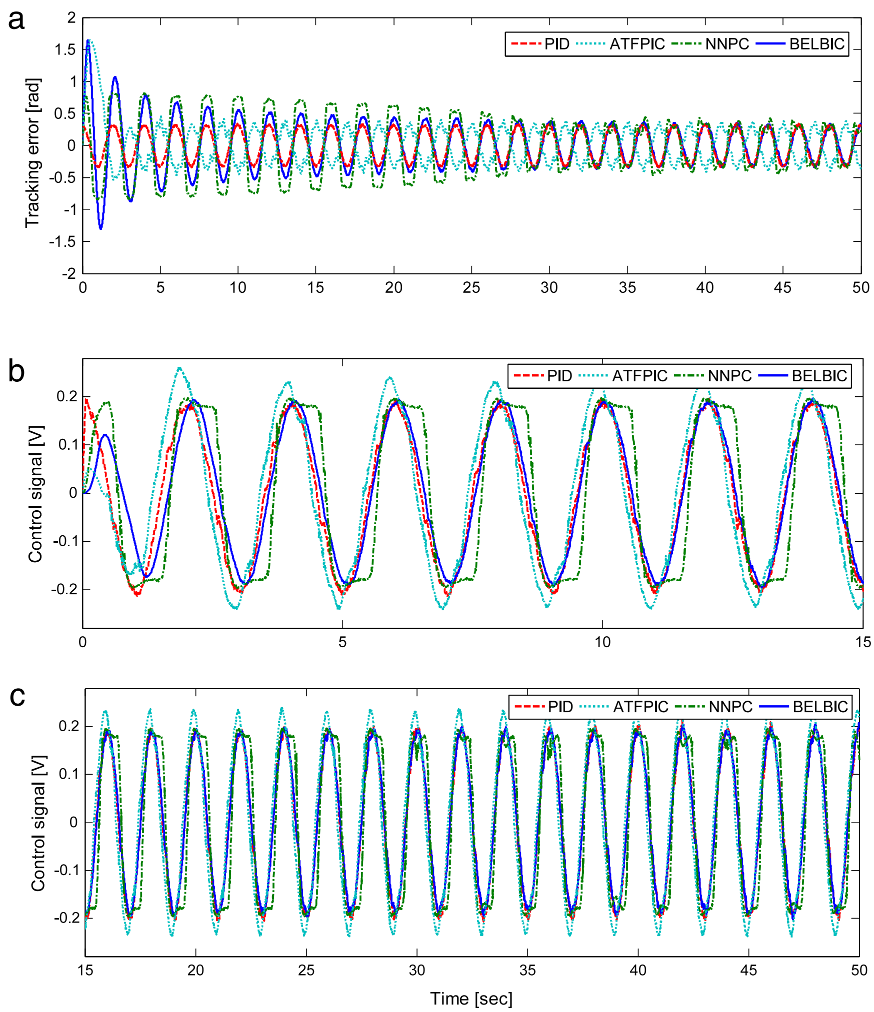

Fig. 8. Experimental position tracking error and control signal for a sinusoidal reference signal with a π (rad/s) frequency and 2 rad amplitude on the hydraulic actuator.

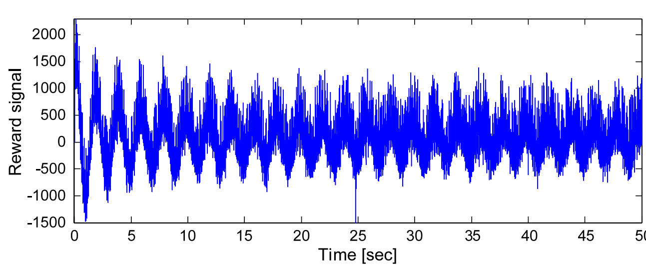

Fig. 9. Experimental stress (reward) signal of the BELBIC during the control process for a sinusoidal reference signal with a π (rad/s) frequency.

parameters is practically impossible. Since the system operates under high pressures, inappropriate selection of a parameter may cause severe damage to the components. Unquestionably the dynamic model provided is simplified and the identification has errors. But the eventual laboratory results given later show that the controller designed based on the model above is robust against uncertainties and parameter variations and has satisfactory control performance.

7.2. Real-time implementation of a BELBIC and comparisons

A series of tests was carried out on the rotary servo-hydraulic actuator under different conditions with the purpose of demonstrating the capabilities of the BELBIC controller. The results of these tests are compared to those of a real-time PID controller, an auto-tuned fuzzy PI controller (ATFPIC), and a neural network predictive controller (NNPC) in exactly similar conditions and with the same amount of feedback. Details regarding the three controllers above are presented in Appendices A–C, respectively.

In Fig. 8, diagrams of tracking error and control signal for the BELBIC, PID controller, ATFPIC, and NNPC have been given, where the reference signal is sinusoidal with a π (rad/s) frequency and 2 rad amplitude. As is clearly understood from Fig. 8(a), the BELBIC's tracking error is visibly higher than that of the PID controller and the NNPC at the beginning of the process. The reason for this is obviously BELBIC's online learning ability. The initial weight values of this controller are zero, and learning the system dynamics is a continual process which occurs over time. As expected, the PID controller like every other linear controller provides acceptable responses in low velocities. Fig. 8(a) fully indicates this situation. The trend of BELBIC's control input variations, during the whole learning process, is notable. The input value is initially zero, and it will reach its ultimate value over time. As seen from Fig. 8(b) and (c), this final value is slightly less than the input control signal of the PID controller. The BELBIC's fairly uniform and smooth control input compared to the other three controllers is of crucial importance in practical applications, especially extreme pressure systems such as EHS systems (Fig. 8(b) and (c)).

How the stress signal varies during the control process is shown in Fig. 9. The stress levels at the beginning of the process are noticeably higher due to high initial tracking error. As Fig. 9 shows,

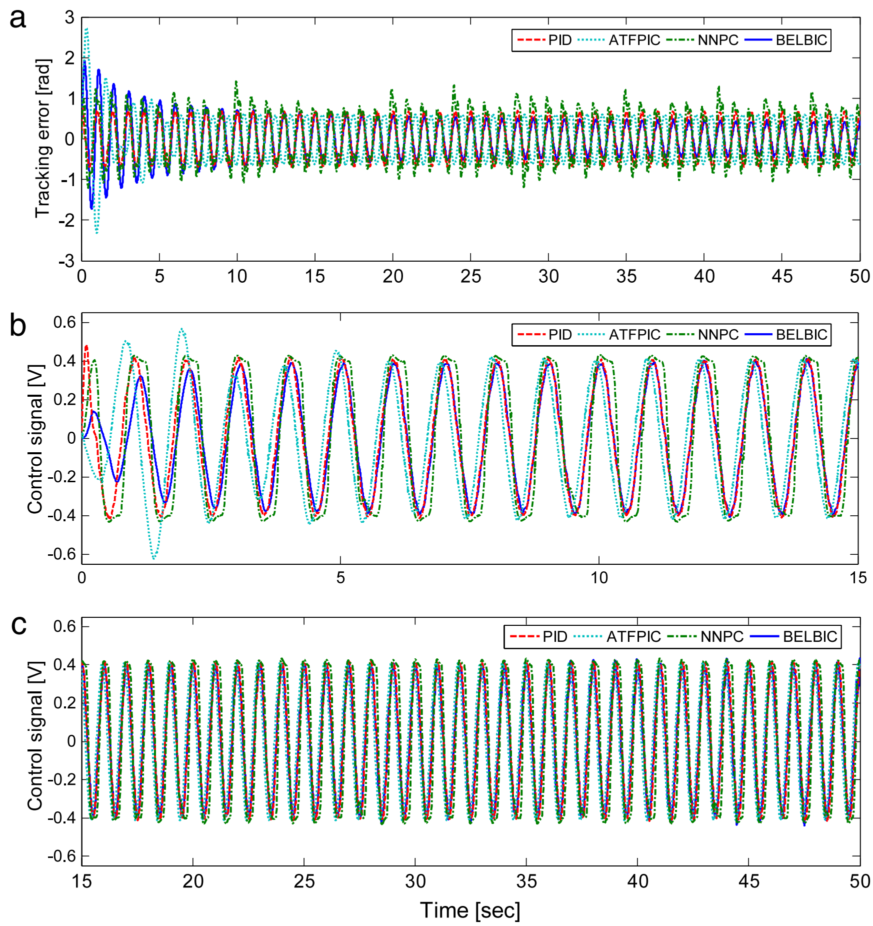

Fig. 10. Experimental position tracking error and control signal for a sinusoidal reference signal with a 2π (rad/s) frequency and 2 rad amplitude on the hydraulic actuator.

the BELBIC has successfully been able to decrease the high levels of stress generated at the beginning of the process.

For an input signal with a sinusoidal reference, 2π (rad/s) frequency, and amplitude of 2 rad for a 50 s time span, the tracking error and control input diagrams are displayed in Fig. 10. As in Fig. 8, the BELBIC and ATFPIC tracking errors when starting implementation are higher than those of the other two controllers (Fig. 10(a)), yet the BELBIC's tracking error falls under the PID controller's constant error after about 15 s, and this descending trend continues until the process ends. The desired signal, when increased, will able the BELBIC to emphasize its swift learning ability, which indicates that the performance of the proposed algorithm is better in higher frequencies. It seems essential to note that this dramatic reduction in tracking error is not only not accompanied by an increase in the BELBIC's control effort but also, as testified in Fig. 10(b) and (c), less control effort is observed in the total process compared to the other three controllers. This issue is another of the BELBIC's beneficial characteristics.

As anticipated, as the frequency of the reference signal increases, the nonlinear nature of the rotary EHS system becomes more evident, thus elucidating the PID controller's disabilities.

In Fig. 11, the BELBIC weights are shown with respect to time. Obviously, the weights of the amygdala reach a constant value, and never decrease, while the weights of the orbitofrontal part, unlike the monotonic amygdala weights, change rapidly to compensate for mismatches between the base system predictions and the received reinforcement signal.

For better deduction of the performance of the four controllers, the time integral of the squared errors (ISE) and the time integral of the squared control efforts (ISU) are given for all four control approaches in Tables 4 and 5. The index values are calculated considering the results from the 15th second to the 50th second. This reasonable consideration is made in order to eliminate the delayed response in the initial learning phase. In this case, the control signal of the BELBIC is better than that of the other controllers, as shown in Tables 4 and 5.

Table 4
Integral performance indices (ISE and ISU) at frequency of π rad/s.

Applied controller	$\int e^2\,dt$	$\int u^2\,dt$
PID	1.8104	0.6591
ATFPIC	2.0851	0.9109
NNPC	5.2366	1.0115
BELBIC	2.4727	0.6337

Table 5
Integral performance indices (ISE and ISU) at frequency of 2π rad/s.

Applied controller	$\int e^2\,dt$	$\int u^2\,dt$
PID	7.7036	2.7812
ATFPIC	6.9124	2.8701
NNPC	13.980	4.2621
BELBIC	3.9918	2.6141

As seen in the tables above, generally the BELBIC demonstrated far better performance than the NNPC; considering the fact that both methods are neuro based, the points below are worth mentioning.

The fairly undesirable results of the NNPC are due to poor training, which can be eliminated if more training data are provided. The high-volume computational burden of this method especially compared to the BELBIC is a major drawback. As explained in Appendix C, this scheme is provided with a pretrained

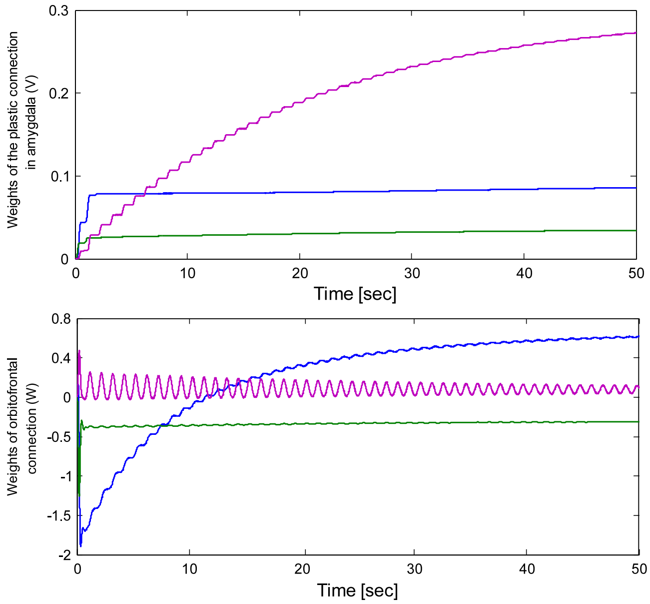

Fig. 11. Weights of the BELBIC through time (at frequency of 2π rad/s).

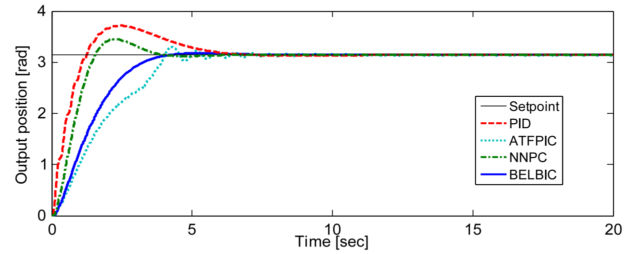

Fig. 12. Experimental step responses of the EHS system.

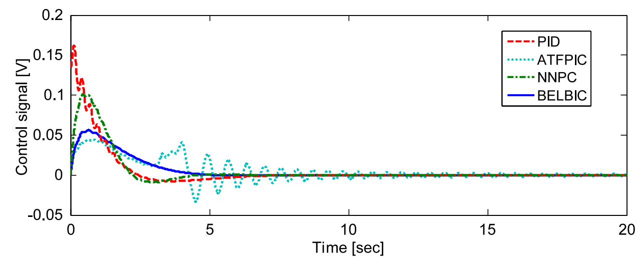

Fig. 13. Experimental control signals for the step reference signal.

neural network (NN) as a model for the process, so in the case of variations in the plant features the algorithm performance would reduce drastically from its optimal status. In order to avoid this problem, an online identification method should be applied to the method, consequently causing an increase in computational load and sophistication of the algorithm.

Finally, the step responses of the system using all controllers in the same conditions are presented in Figs. 12 and 13. In industrial control applications it is common to specify an overshoot of 8–10%. In many situations it is desirable, however, to have an overdamped response with no overshoot. Comparing the system responses for different controllers indicates that the BELBIC, with appropriate settling time and rise time, completely satisfies the desirable performance. The overshoot of the control signal is also of particular importance in industrial applications. The BELBIC, displaying less overshoot and undershoot, did not make a control effort that was any greater than that of the other controllers.

8. Conclusion

In this paper, modeling, identification, and position controlling of a laboratorial EHS system that is dynamically nonlinear and time varied has been done. The performance of the proposed controller has been compared to that of a real-time PID controller, an NNPC, and an ATFPIC in completely similar conditions. Experiments carried out indicate that the BELBIC's swift learning ability reduced the tracking error effectively. It is also concluded that the BELBIC produces a smooth and uniform control signal in addition to efficient energy consumption. It goes without saying that these advantages have not caused a significant increase in the computational burden. The main shortcoming of model-free learnable controllers without prior knowledge of the system dynamics is that, in early phases of the learning process, they may experience poor performance due to the production of an incorrect control signal both in direction and magnitude. Future research can focus on a hybrid control to solve this problem and accelerate the learning procedure. Undoubtedly, the proposed approach is not an optimal solution; however, with simple implementation, reasonable computational effort, a straightforward control structure, and without an accurate description of system dynamics, this method proves to be both efficient and acceptable for complex industrial applications.

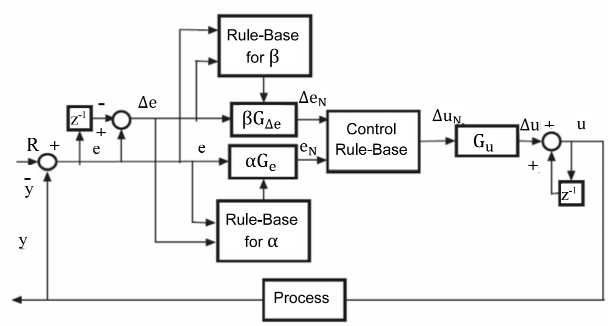

Fig. B.1. Block diagram of the ATFPIC scheme [27].

Appendix A

It should be noted that PID gain tuning has been optimized by applying Simulink®Design Optimization™ based on the gradient descent method with the active set algorithm to achieve satisfactory performance. Finally, after optimization, the PID gains were calculated as follows: $K_p = 0.63$, $K_i = 0.27$, and $K_d = 0.04$.

Appendix B

The block diagram of the proposed auto-tuned fuzzy PI controller is shown in Fig. B.1. In this method, the input scaling factors are tuned online by some updating factors whose values are fuzzy rule base with the error and change in error as inputs according to the required controlled process.

In Fig. B.1, α and β are the updating factors for incremental change in e and Δe, which are computed online based on fuzzy logic reasoning using the error and change in error at each sampling time. For a fuzzy PI-type controller, Δu is the incremental change in controller output, which is determined by the rules of the following form: if e is E and Δe is ΔE, then Δu is ΔU. Also, the initial values of the scaling factors $G_{\Delta e}$, G_e, and G_u are determined by simulations in order to achieve satisfactory responses.

All membership functions (MFs) for controller inputs (i.e., e and Δe) and incremental change in controller output (i.e., Δu) are defined on the common normalized domain $[-1, 1]$. The membership functions are shown in Fig. B.2. The MFs for α are defined on the range $[-0.5, 1.5]$ but with two fuzzy sets, small and

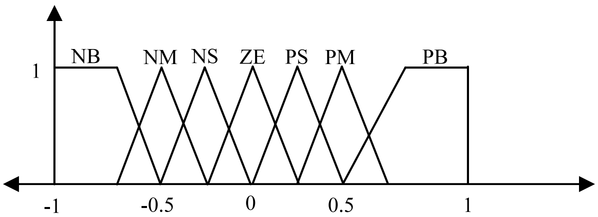

Fig. B.2. MFs for e, Δe and Δu.

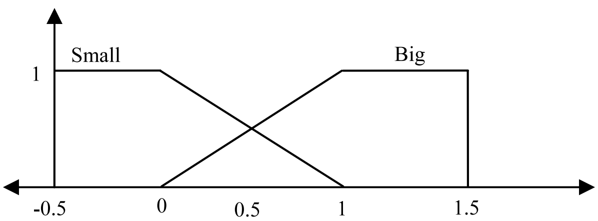

Fig. B.3. MFs for gain updating factor α.

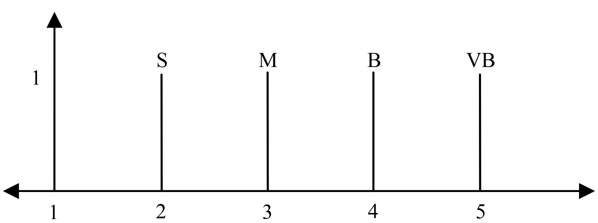

Fig. B.4. MFs for gain updating factor β.

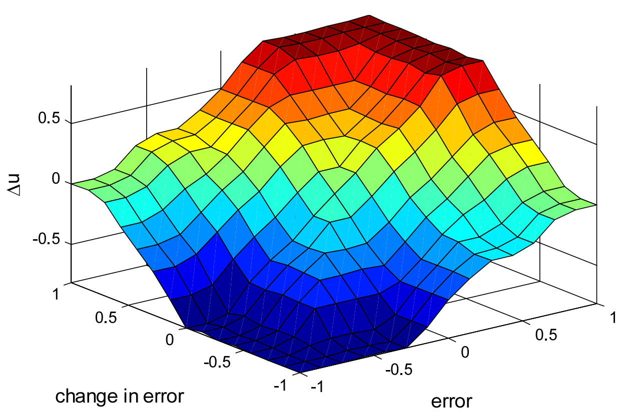

Fig. B.5. Fuzzy surface of Δu.

big, and the MFs of β, corresponding to the singleton fuzzy sets, varies from [1,5], as shown in Figs. B.3 and B.4.

The Δu fuzzy surface is shown in Fig. B.5 and the fuzzy surfaces of α and β are given in Figs. B.6 and B.7. The presented fuzzy surfaces are actually fuzzy rule base which have been specifically designed for the current EHS system.

Appendix C

The block diagram of the proposed neural network predictive controller (NNPC) is shown in Fig. C.1.

In this method, two independent neural networks are applied: one is a model of the system, which predicts the plant response, and the other is used as the controller, which functions by

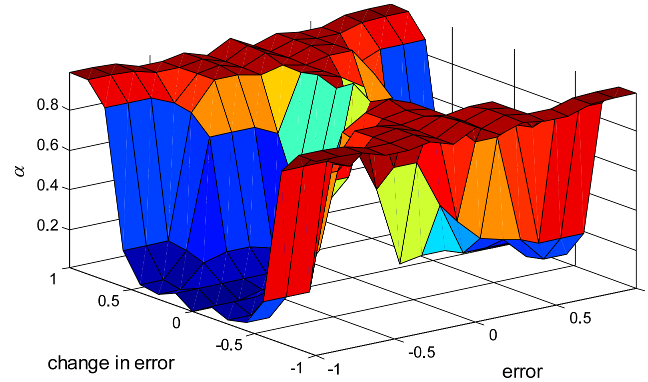

Fig. B.6. Fuzzy surface of α.

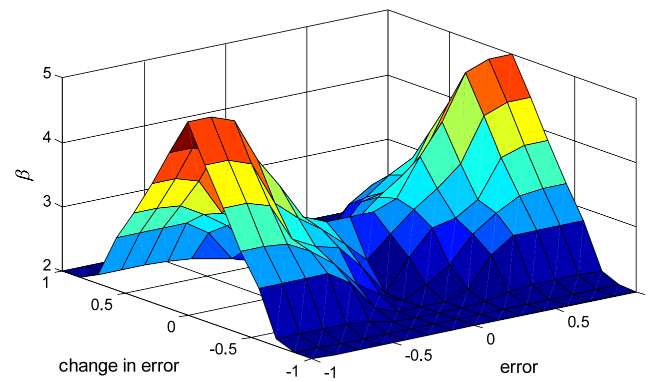

Fig. B.7. Fuzzy surface of β.

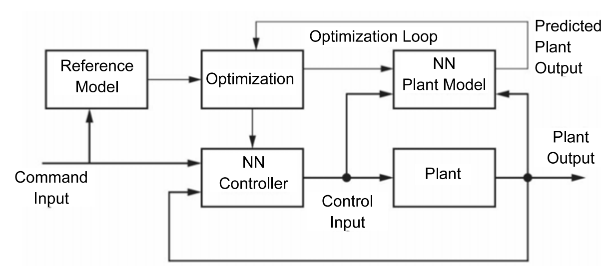

Fig. C.1. Neural network predictive control (NNPC) scheme [28].

minimizing the following cost function:

$$J = \sum_{j=N_1}^{N_2} (y_r(k+j) - y_m(k+j))^2 + \rho \sum_{j=1}^{N_u} (u'(k+j-1) - u'(k+j-2))^2, \qquad (C.1)$$

where N_1, N_2, and N_u define the horizons over which the tracking error and the control increments are evaluated. The u' variable is the tentative control signal, y_r is the reference response, and y_m is the network model response. The ρ value determines the contribution that the sum of the squares of the control increments has on the performance index.

The training process of the neural identifier is discussed in detail in [28], where the controller parameters are set to $N_1 = 0, N_2 = 10$, $N_u = 3$, and $\rho = 0.01$, with a sampling interval of 0.001 s for the current EHS system.

References

[1] Merritt HE. Hydraulic control systems. New York: John Wiley & Sons; 1967.
[2] Lim TJ. Pole placement control of an electro-hydraulic servo motor. In: Proc. 2nd int. conf. power electron. drive syst., part 1, vol. 1. May 1997. p. 350–6.
[3] Fink A, Singh T. Discrete sliding mode controller for pressure control with an electrohydraulic servovalve. In: Proc. IEEE int. conf. control appl., vol. 1. 1998. p. 378–82.
[4] Chen H-M, Renn J-C, Su J-P. Sliding mode control with varying boundary layers for an electro-hydraulic position servo system. Int J Adv Manuf Technol 2005; 26:117–23.
[5] Fales R, Kelkar A. Robust control design for a wheel loader using H-infinity and feedback linearization based methods. ISA Trans 2009;48(3):312–20.
[6] Kaddissi C, Kenné J-P, Saad M. Identification and real-time control of an electrohydraulic servo system based on nonlinear backstepping. IEEE/ASME Trans Mechatron 2007;12(1):12–22.
[7] Milić V, Šitum Ž, Essert M. Robust H-infinity position control synthesis of an electro-hydraulic servo system. ISA Trans 2010;49(4):535–42.
[8] Lucas C, Milasi RM, Araabi BN. Intelligent modeling and control of washing machine using locally linear neuro-fuzzy (LLNF) modeling and modified brain emotional learning based intelligent controller (BELBIC). Asian J Control 2005; 8(4):393–400.
[9] Sheikholeslami N, Shahmirzadi D, Semsar E, Lucas C, Yazdanpanah MJ. Applying brain emotional learning algorithm for multivariable control of HVAC systems. Int J Intell Fuzzy Syst 2006;17(1):35–46.
[10] Rouhani H, Jalili M, Araabi BN, Eppler W, Lucas C. Brain emotional learning based intelligent controller applied to neurofuzzy model of micro-heat exchanger. Expert Syst Appl 2007;32:911–8.
[11] Mehrabian AR, Lucas C, Roshanian J. Design of an aerospace launch vehicle autopilot based on optimized emotional learning algorithm. Cybern Syst: Int J 2008;39(April):284–303.
[12] Sharbafi MA, Lucas C, Toroghi Haghighat A, Ghiasvand OA, Aghazade O. Using emotional learning in rescue simulation environment. Trans Eng, Comput Technol 2006;13(May):333–7.
[13] Jamali MR, Arami A, Hosseini B, Moshiri B, Lucas C. Real time emotional control for anti-swing and positioning control of SIMO overhead travelling crane. Int J Innovative Comput, Inf Control 2008;4(9):2333–44.
[14] Rahman MA, Milasi RM, Lucas C, Araabi BN, Radwan TS. Implementation of emotional controller for interior permanent-magnet synchronous motor drive. IEEE Trans Ind Appl 2008;44(5):1466–76.
[15] Neese R. Emotional disorders in evolutionary perspective. British J Med Psychology 1998;71:397–415.
[16] Fellous JM, Armony JL, LeDoux JE. In: Arbib MA, editor. The handbook of brain theory and neural networks. 2nd ed. Emotional circuits and computational neuroscience, Cambridge (MA): The MIT Press; 2002.
[17] Inoue K, Kawabata K, Kobayashi H. On a decision making system with emotion. In: 5th IEEE int. workshop robot human commun. 1996. p. 461–5.
[18] Bay JS. Behavior learning in large homogeneous populations of robots. In: IASTED int. conf. artificial intell. soft comput. 1997. p. 137–40.
[19] Miyazaki K, Araki N, Mogi E, Kobayashi T, Shigematsu Y. Brain learning control representation in nucleus accumbens. In: Second int. conf. knowl. intell. electron. syst. Australia; 1998. p. 21–3.
[20] Moren J, Balkenius C. A computational model of emotional learning in the amygdala: from animals to animals. In: Proc. 6th int. conf. simul. adaptive behavior. Cambridge (MA): The MIT Press; 2000. p. 383–91.
[21] Moren J. Emotional and learning—a computational model of the amygdala. Ph.D. dissertation. Lund (Sweden): Dept. Cognitive Stud., Lund Univ.; 2002.
[22] Lucas C, Shahmirzadi D, Sheikholeslami N. Introducing BELBIC: brain emotional learning based intelligent controller. Int J Intell Autom Soft Comput 2004;10(1):11–22.
[23] Shahmirzadi D, Langari R. Stability of amygdala learning system using cell-to-cell mapping algorithm. In: Proc. IASTED int. conf. intell. syst. control. Cambridge (USA); 2006.
[24] Ayalew B, Kulakowski BT. Modeling supply and return line dynamics for an electrohydraulic actuation system. ISA Trans 2005;44(3):329–43.
[25] Jelali M, Kroll A. Hydraulic servo-systems: modelling, identification, and control. Springer; 2003.
[26] Astrom KJ, Wittenmark B. Adaptive control. Boston (MA): Addison-Wesley; 1995.
[27] Chopra S, Mitra R, Kumar V. Auto tuning of fuzzy PI type controller using fuzzy logic. Int J Comput Cognition 2008;6(1):12–8.
[28] Hagan MT, Demuth HB. Neural networks for control. In: Proc. American control conf. San Diego (CA); 1999. p. 1642–56.